Cargo transport by catchbonded motors in optical trapping assays

Naren Sundararajan[1,2,*], Sougata Guha[3,*], Sudipto Muhuri[1,†], Mithun K. Mitra[3,‡]
[1] *Department of Physics, Savitribai Phule Pune University, Pune, India*
[2] *Martin A. Fisher School of Physics, Brandeis University, Waltham, MA, USA*
[3] *Department of Physics, IIT Bombay, Mumbai, India*
[*] *These authors contributed equally*
[†] *sudipto@physics.unipune.ac.in*
[‡] *mithun@phy.iitb.ac.in*

Experiments performed using optical trapping assays constitute an important means of accurately measuring the molecular forces generated by molecular motor proteins. We investigate, using theory and stochastic simulations, the transport properties of cargo transported by dynein molecular motors - both singly and in teams - in a harmonic potential, which mimics the variable force experienced by cargo in an optical trap. In particular, we investigate the role of the dynein catch bond in altering the transport properties of cellular cargo - as quantified through the biologically relevant measures of run lengths, detachment forces and first passage time. Our results suggest that even for cargo transported by a single motor, catchbonding may play a role depending on the force scale which marks the onset of the catch bond. For cargo transported by multiple motors, emergent collective effects due to catchbonding can result in non-trivial re-entrant phenomena for average first passage times and detachment forces as function of the stall force and the motor velocity.

I. INTRODUCTION

The process of intracellular transport involves the collective action of many motor proteins [1–13]. Unravelling the underlying physical mechanism by which individual motor properties translates into their collective behaviour is of crucial importance for understanding the observed transport characteristics of the cellular cargo. Multiple theoretical and simulation studies have investigated the transport characteristics of cargo in the presence of a constant load force [14–16]. Optical trap assays have provided the means to measure and quantify force generated by individual motors at the scale of single-molecule resolution [17, 18]. Since the restoring force experienced by a motor increases with the distance of the cargo from the trap center, optical traps should be modelled as a variable force ensemble, with the motion being arrested when the cargo has travelled a sufficient distance such that the force on the motors exceeds the stall force. Using this optical trap setup to track the movement of organelle under *in-vivo* conditions or latex bead driven by molecular motors for *in-vitro* experiments, has enabled systematic calibration of the motility characteristics of the transported cellular cargo on variation of individual motor properties [18, 19]. These optical trap based experiments have provided wealth of information about individual motor properties and they have also provided insight how the individual motor properties fashion their collective behaviour. At the level of individual motors, these experimental studies have provided strong indications of *catchbonded* nature of dynein binding to the microtubule (MT) filament [20]. Specifically it has been observed that the lifetime of dynein bond to the MT actually increases with increase in opposing load force [17, 18]. These experiments have also served to highlight how the structural differences of kinesin and dynein motors manifests as divergent collective transport characteristics of cellular cargo that is carried by these motor proteins. In particular, it has been observed that while team of dynein can work in unison to generate large forces inside the cell, and resist detachment from microtubule (MT) filament, multiple kinesin motors in presence of opposing load fail to sustain load force and quickly detach from the MT filament [18]. One hypothesis which has been proposed in this context is that for organelle transport by dynein, the cooperative nature of transport arises as a consequence of the load being shared equally among the motors [18, 19]. It has been argued that in fact the *catchbond mechanism* at play for dynein bond under load force leads to increased bond lifetime, which in turn allows the trailing motors to catch up and share the opposing load force [18, 19].

While,it was thought that the primary functional role of the biological catchbond was restricted to improving surface adhesion properties of bacteria and cell when subjected to external forces or flow field [21], many recent theoretical studies have indicated a much wider array of functional role of the biological catchbonding in intracellular processes ranging from regulating intracellular transport [13, 15, 22] to generating oscillations in muscle fibres and mitotic spindles during cell division [23]. Thus it is imperative to understand the underlying mechanism which governs the collective behaviour of cathbonded dynein motors. In this context, experiments using optical trap assay provides a useful means of not only investigating the role of catchbond in dynein motors on intracellular properties but it may also be used for systematically studying the effects of variation of the single motor properties such as the stall force and the motor velocity on the overall motility characteristics of the transported cellular cargo. For instance, it has been observed for *in-vivo* experiments that complexing dynein

with dynactin, not only modulates the stall force of the motor and unbinding rate of dynein from filament, but it also manifests as modified processivity of these motors [24].

In this paper we seek to understand the role of catch-bond in mediating transport of cellular cargoes. To this end, we model the cargo being transported by multiple dynein motors in an optical trap. We perform stochastic simulation of cellular cargo being transported by dynein motors while being subject to the restoring force arising due to the harmonic potential of the optical trap and analyse the effect of single motor properties, e.g., catch-bond strength, stall force and motor stiffness on different transport characteristics of the transported cargo that we quantify in terms first passage time and detachment force (the force exerted on the cargo at the time of its detachment from MT filament).

II. MODEL AND METHODS

We model the transport of a cellular cargo that is subjected to force due to the translational motion of motors that are attached to cargo and walk on microtubule filaments as well as an opposing restoring force arising due to the harmonic potential of the optical trap. The motors themselves stochastically (un)bind from the MT filament in a force dependent manner. As far as the unbinding characteristics of the motors are concerned, while the unbinding rate of non-catchbonded motors are an increasing function of the force they are subjected to, for catchbonded dynein motors, the unbinding force is a decreasing function of the force. We incorporate the catchbonded nature of dynein motors using Threshold Force Bond deformation (TFBD) model [13, 15] and perform stochastic simulation to study the essential differences arising in transport characteristics due to the catchbonding behaviour of the motors. First we study the characteristics of transport of a cargo by single motor, delineating the differences arising on account of the catchbonded nature of the unbinding process. Next, we study the emergent transport characteristics due to the collective action of multiple motors. Allowing for stochastic load sharing of the cargo transported by the motors, we analyze the individual cargo trajectory and characterize the collective transport properties of the cellular cargo using the distributions associated with the measures of detachment force and the first passage time of cargo unbinding from filament. By tuning the strength of catchbond, we also systematically investigate the role of catchbond in facilitating the cooperative mechanism of sharing load between the motors.

A. Theoretical estimates of First passage time for single motor

For transport of a cellular cargo by a single motor, the cargo is subjected to pulling force of a single motor that is attached to the underlying microtubule filament and an opposing restoring force arising from the potential due to optical trap potential. The effect of the optical trap on the cellular cargo is modelled as a harmonic potential of the form $V_t = \frac{1}{2}k_t x_c^2$, where k_t is the spring constant associated with the optical trap and x_c is the displacement of the cargo from the center of the trap. The motor is also modelled as a harmonic spring, whose effective spring constant is k_m. We assume that the motor binds to a random binding site on the filament within its rest length distance (l_o) from the trap center (i.e. $-l_o \leq x_m(t=0) \leq l_o$). The rest length of the motor is defined as the maximum extension of the motor from the cargo position for which the motor experiences no load. The instantaneous position of the cargo $x_c(t)$ is determined by balancing the counteracting forces exerted by the optical trap and the motors. The force balance condition reads as,

$$k_t x_c = \Theta(x_m - x_c - l_o) k_m (x_m - x_c) \tag{1}$$

where x_m is the displacement of the motor with respect to the center of the optical trap, and the Heaviside theta function $\Theta(x) = 1$ if $x > 0$ and zero otherwise. It follows that, for a single motor, the force exerted on the motor is non-zero only when the motor distance from optical trap is greater than its rest length ($x_m > l_o$). The cargo position can be expressed as $x_c = \Theta(x_m - x_c - l_o)\left(\frac{k_m}{k_m+k_t}\right) x_m$. Consequently, the cargo velocity, v_c, can be expressed in terms of the motor velocity, v_m as,

$$v_c = \Theta(x_m - x_c - l_o)\left(\frac{k_m}{k_m + k_t}\right) v_m \tag{2}$$

We assume a linear force- velocity relation for the motor, with motor velocity $v_m = v_o(1 - f/f_s)$ [14], where v_o is single motor velocity at zero load force, f is the force exerted on the motor and f_s is the stall force of the motor. Then, as per Eqn.(2), the instantaneous force f exerted on the motor is related to the instantaneous cargo position $x_c(t)$ and it can be expressed in terms of the time interval t for which the motor is bound to the MT filament as ,

$$f(t) = k_t x_c(t) = \Theta(v_o t - l_o) f_s \left[1 - \exp\left(-\frac{k_t k_m (v_o t - l_o)}{(k_t + k_m) f_s}\right)\right] \tag{3}$$

where the Θ function is non-zero only for t greater than the mean time taken by the motor to walk beyond its rest length.

The unbinding rate of the motor from the filament, ϵ, depends on the force f exerted on the motors. For non-catchbonded motors such as kinesin, the unbinding rate

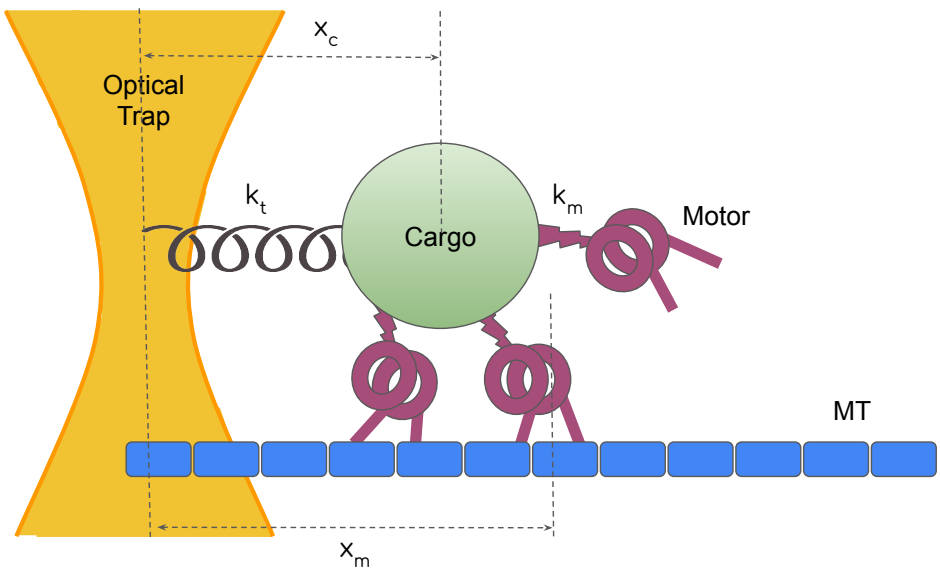

FIG. 1. Schematic of motor driven cargo transport on a microtubule (MT) filament in an optical trap. The optical trap and the motors are denoted as a harmonic springs with spring constants k_t and k_m respectively. The positions of the cargo and the motors from the optical trap centre is denoted by x_c and x_m respectively.

increases exponentially with the load force - a characteristic of *slip bond*, such that

$$\epsilon(f) = \epsilon_o e^{f/f_k} \tag{4}$$

where, f_k is the characteristic detachment force for kinesin motor.

In contrast, for catchbonded dynein motors, it has been observed that beyond certain load force, the unbinding rate is a decreasing function of the force - a signature of catchbonding behaviour exhibited by dynein motors [20]. The structure of dynein motor comprises of a linker-stem domain which attaches to the cellular cargo and the flexible MT-binding domain. It is hypothesized that a load force leads to contraction of the AAA domain which in turn causes allosteric deformation of the MT-binding domain resulting in catchbonding behaviour exhibited by dynein motor [19]. We denote the corresponding threshold force at which catchbonding sets in dynein as f_m. It is worthwhile to point out that f_m need not necessarily be same as the stall force f_s of the motors. However in-vitro experiments with single cytoplasmic dynein motor suggest that f_s and f_m are of comparable magnitude [20].The unbinding rate for single dynein motor can be modelled and fitted using a phenomenological TFBD model [15] which reproduces the observed experimental unbinding rates of cytoplasmic dynein motor. Within the framework of the TFBD model, the unbinding rate of single dynein motor can be expressed as,

$$\epsilon(f) = \epsilon_o \exp[-E_d(f) + f/f_d\ ] \tag{5}$$

where f_d is the characteristic detachment force of dynein motor in the slip region ($f < f_m$). The deformation energy E_d represents the influence of catchbond behaviour, which sets in when $f > f_m$, and is expressed as [15],

$$E_d(f) = \Theta(f - f_m)\ \alpha \left[1 - \exp\left(-\frac{f - f_s}{f_o}\right)\right] \tag{6}$$

where, the parameter α is a measure of catchbond strength, and f_o is a parameter associated with the force scale corresponding to the deformation energy due to catchbond.

We define $S(t)$ as the *Survival probability* distribution of the cellular cargo i.e., the probability that the cargo remains attached to the filament (through the bound motor) after time t, starting from the initial position of the optical trap center at time $t = 0$. Then for a small time interval Δt, $S(t+\Delta t) = S(t)[1-\epsilon(f)\Delta t]$ and corresponding time evolution of $S(t)$ is,

$$\frac{dS}{dt} = -\epsilon(f)S \tag{7}$$

which yields a solution of $S(t)$, which has the general form,

$$S(t) = \exp\left[-\int_0^t \epsilon dt'\right] \tag{8}$$

For non-catchbonded motors, we have $\epsilon = \epsilon_o e^{k_t x_c/f_k}$. Using Eq.(3), we obtain,

$$\epsilon(t) = \epsilon_o \exp\left[\Theta(v_o t - l_o)\frac{f_s}{f_k}\left(1 - e^{-K(v_o t - l_o)}\right)\right] \tag{9}$$

where $K = \frac{k_t k_m}{(k_t+k_m)f_s}$. The probability distribution of the survival time, $S(t)$, can then be obtained by substituting the expression for ϵ obtained in Eq.(9) in the integral form of Eq.(8). Once the distribution of survival probability is obtained, the *First passage time* distribution, $F(t)$, can easily be calculated from Eq.(7) using the relation $F(t) = -\frac{dS}{dt}$. For the catchbonded motors, the form of the unbinding rate is obtained from Eq.(5) and Eq.(6), which in turn is substituted in the integral form of Eq.(8), to obtain the survival probability distribution and hence the probability distribution of the first passage time. Once we obtain the first passage time distribution, we can calculate the detachment force distribution, $P(f)$, using the following expression -

$$P(f) = \frac{\int_0^t f(t')F(t')dt'}{\int_0^t F(t')dt'} \tag{10}$$

B. Simulation of cargo trajectories: Single motor case

In the stochastic simulation, the movement of the cargo away from the trap center is tracked. The initial position of the cargo coincides with the minima of the optical trap potential, i.e., $x_c^{initial} = 0$. The motor is modelled by a harmonic spring with a stiffness k_m and rest-length l_o [20]. Hence due to the force balance condition, cargo displacement occurs whenever the motor is stretched beyond its rest length. We start with motor bound anywhere in a linear region between $x_c - l_o$ and $x_c + l_o$ with equal probability. The instantaneous position of the cargo is determined by the force balance condition in Eq.(1). The force on each motor, f is a stochastic quantity which is determined by its position relative to the cargo as $f = -k_m(x_m - x_c - l_o)$. In any time interval Δt in the simulation, the motor either attempts to detach with a rate ε, or it attempts a step forward by a step-size d, resulting in the displacement of the cargo position. The forward step succeeds with a probability $p = k_{step}\Delta t = \frac{v_m(f)}{d}\Delta t$, where the $v_m(f)$ is the force-dependent motor velocity. If the motor detaches, the run comes to an end.

For the purpose of our simulation, we choose the stiffness of motor $k_m = 0.2pN/nm$ [26], trap stiffness $k_t = 0.02pN/nm$ [26] and the rest-length l_o for dynein to be $55nm$ [27]. We simulate the trajectories and obtain the statistical measures of by generating over 5000 runs of the samples.

C. Simulation of Cargo trajectories: Multiple motor case

In the case of multiple motors, motors can now also bind back to the filament as long as there is at least one motor keeping the cargo bound to the filament. When the position of the individual motor, x, with respect to the cargo position exceeds their rest length l_o, the motors exerts a force $f = k_m(x - x_c - l_o)$. Thus the cargo is subjected to pulling force of attached motors that are stretched beyond the rest length and a restoring force due the optical trap, which is simply equals to $-k_t x_c$. The instantaneous position of the cargo $x_c(t)$ is determined by the instantaneous force balance condition achieved by the counteracting forces on the cargo due to the collective action of many attached motors which are stretched beyond their rest length and the force due to the optical trap potential. This force balance condition reads as,

$$k_t x_c = \sum_{i=1}^{N} \Theta(|x_i - x_c| - l_o)k_m(x_i - x_c - l_o)$$

where, x_i is the instantaneous position of the i-th motor that is attached to the filament and N is the total number of motors attached to the cargo.

Like for the case of transport by single motor, we assume a linear force- velocity relation for the motor [14]. So that the velocity of the individual motors are related to the force f exerted on the individual motor as,

$$v_m = v_o(1 - f/f_s) \tag{11}$$

when, $0 < f \leq f_s$. In case of assisting load ($f \leq 0$), we assume that the motors move with the constant load-free velocity v_o [14]. For opposing load higher than the stall force (f_s), the motors are stalled and do not move.

Similar to the case of cargo transported by non-catchbonded single motor, individual motors in a team exhibits *slip behaviour* and the corresponding unbinding rate of the individual motor from the filament, k_u, increases exponentially with load force f following Eq.(4). For catchbonded motors, the unbinding rate is a decreasing function of the force beyond the threshold force of the motor and we take the explicit form of the unbinding rate of these motors to be identical to the TFBD model which are same as Eq.(5) and Eq.(6).

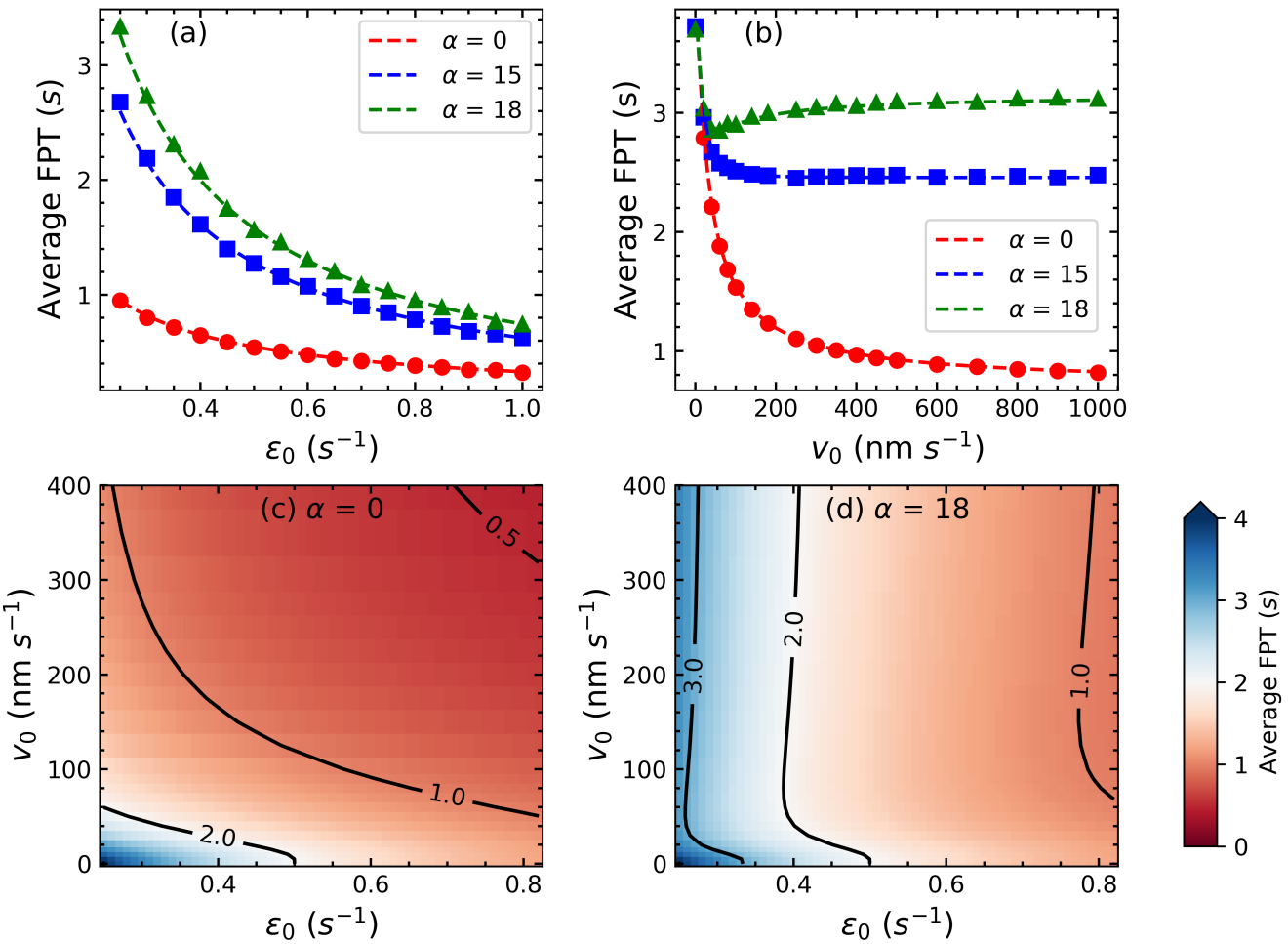

FIG. 2. First passage time for single motor cargo transport. Panels (a) and (b) show the comparison between simulation-generated (dots) and analytically calculated (solid lines) First Passage time t for a single motor. In this case, the motor has a threshold force smaller than its stall force. Red curves correspond to slipbond ($\alpha = 0\ k_BT$) , blue curves to catchbond ($\alpha = 15\ k_BT$) and green curves to Strong catchbond ($\alpha = 18\ k_BT$). Panels (c) and (d) show contour maps of variation of FPT with ϵ_o and v_o simultaneously and demonstrate the appearance of a re-entrant under the influence of catch-bond ($\alpha = 18\ k_BT$). The parameter values used are as follows : $\pi_o = 1.6$ s^{-1}, $\epsilon_o = 0.27$ s^{-1}, $l_o = 0$ nm, $v_o = 362$ nm s^{-1}, $f_s = 1.1$ pN, $f_d = 0.67$ pN, $f_m = 0.5$ pN, $f_o = 7$ pN, $k_t = 0.02$ pN nm^{-1}

III. RESULTS

A. Cargo transport by single motor

1. *First passage properties*

In order to investigate the effect of catchbonded behaviour exhibited by a dynein on the transport characteristics of a cargo being transported by a single dynein motor in an optical trap, we focus on experimentally accessible measures of first passage time (FPT) and detachment force distribution of the cargo. First passage time is the total time the cargo remains bound to the MT before motor that tethers it to the filament, unbinds. The detachment force is the force exerted on the cargo at the time of unbinding of the motor from the MT filament. For a cargo transported by a single motor in an optical trap, if the force at which catchbonding behaviour sets in for the motor, f_m, is same or greater than the single motor stall force f_s, then both FPT and detachment force would be insensitive to the catchbonded nature of the dynein since the optical trap can only access force scale up to f_s for a single motor. In principle, the allosteric deformation force scales which results in catchbonding behaviour in dynein need not be same as the stall force of these motors. We thus explore the regime wherein, $f_m < f_s$, in order to study the potential impact of catchbonding on cargo transport by single motor. For a stall force of $f_s = 1.1pN$ [4, 22, 28], we report results for a choice of $f_m = 0.5pN$.

We characterise the First Passage Time (FPT), and

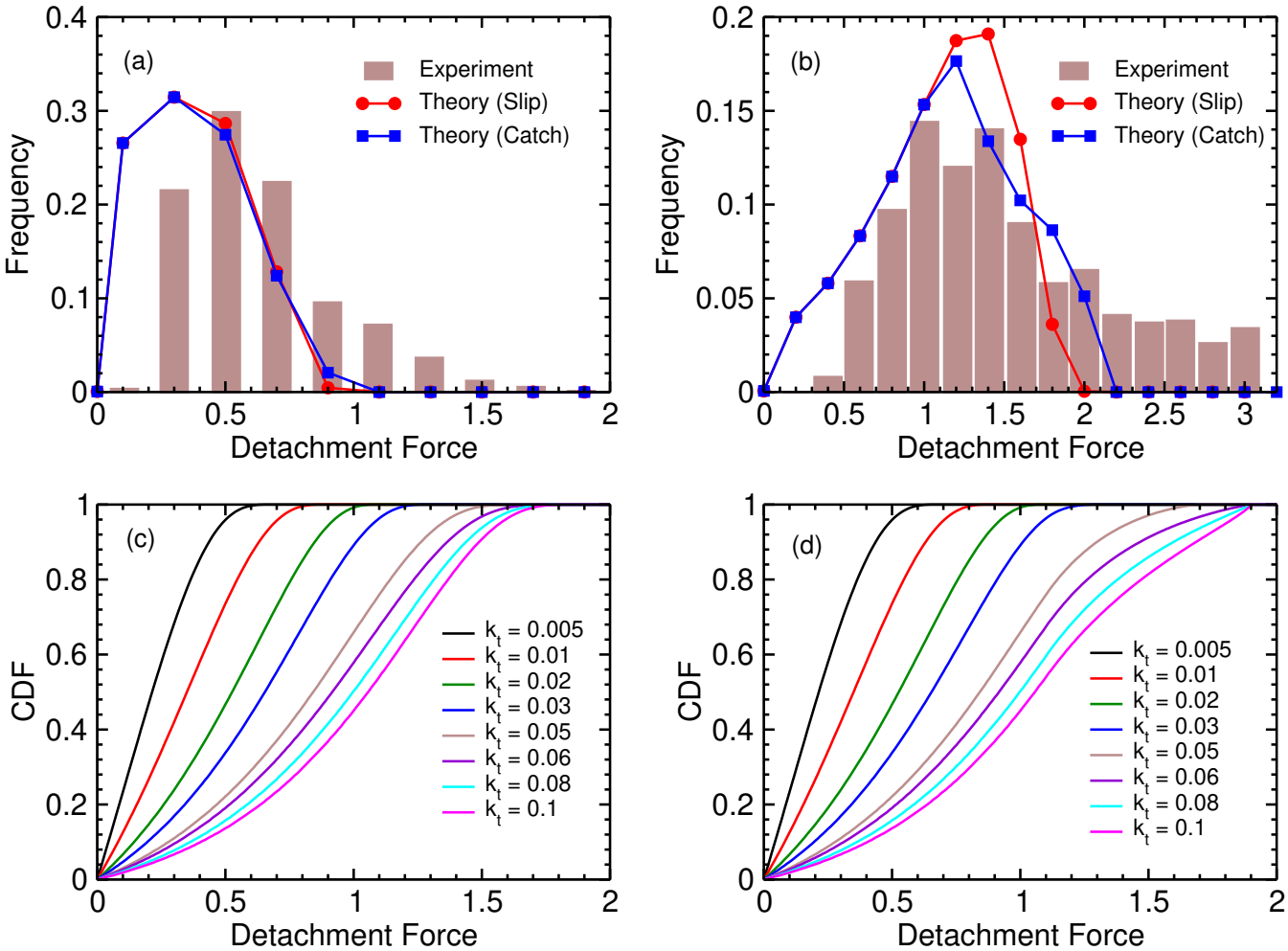

FIG. 3. Panel (a) and (b) compares detachment force distribution between theory and experiment [25] for trap stiffness $k_t = 0.01$ pN/nm and $k_t = 0.1$ pN/nm respectively. Panel (c) shows theoretical estimates of cumulative distribution function (CDF) of detachment force for different trap stiffness in absence of catchbond while panel (d) shows the same in presence of catchbond. The parameter values used are as follows : $\epsilon_o = 6$ s^{-1} [25], $v_o = 540$ nm s^{-1} [25], $l_o = 0$ nm, $f_d = 0.67$ pN, $f_o = 7$ pN, $\alpha = 18$ (for catchbond). In panel (a) $f_m = 0.5$ pN while in all other panels $f_m = 1.1$ pN. Variation of stall force (f_s) of motor with trap stiffness is considered as following - f_s =0.7 pN for k_t =0.005 pN nm^{-1}, f_s =0.9 pN for k_t =0.01 pN nm^{-1}, f_s =1.1 pN for k_t =0.02 pN nm^{-1}, f_s =1.3 pN for k_t =0.03 pN nm^{-1}, f_s =1.7 pN for k_t =0.05 pN nm^{-1} and f_s =1.9 pN for k_t ≥0.06 pN nm^{-1}.

investigate how different motor parameters such as the unbinding rate and motor velocities affect the FPT both in presence and in absence of catchbond.

Fig. 2(a) demonstrates that the first passage time for the bound-state of a cargo driven by a single motor decreases monotonically with an increasing principal unbinding rate ϵ_o. Further, the blue and green curves demonstrate that for the case of catchbonded motors, the first passage time increases with catch-bond strength for the given range of unbinding rates. Thus, a key tenet of catchbonded motors is improved persistence in the bound state of the cargo. The standard response for motors transporting cargo against a harmonic force, is a decrease in persistence of the bound state as the cargo travels away from the trap-center. This is demonstrated in Fig. 2(b) by the red curve where average first passage time decreases monotonically with the principal velocity parameter. This simply indicates that, with higher velocities, motors have a tendency to unbind faster as they venture into regions that elicit a stronger trap force. However, the blue and green curves demonstrate that catch-bond counters this effect by decreasing the unbinding rate at these higher force regimes. There is an initial decrease in first passage time in the small v_o limit as the cargo dynamics is not very likely to trigger a catchbond response at these velocities. However, at a sufficiently higher velocity, the probability of triggering catchbond grows and it is more typical for the cargo's bound state to have higher persistence, leading to an increase in First passage time with v_o. We identify this re-entrant, exclusively, as

a consequence of catch-bond. The contour-lines in Fig 2(d), further show that this behavior is robustly exhibited for a wide range of principal unbinding rate ϵ_o, in contrast with Fig. 2 (c) for slip-bond where it is completely absent.

2. Comparison with experiments

Recent optical trap experiments on human dynein purified from human embryonic kidney (HEK) 293 cells have shown that for this weakly processive mammalian dynein, for weak trap stiffness, the motor unbinds before it experiences the true stall force [25]. By performing experiments systematically for different values of trap stiffness, they show that the observed stall forces depend on the trap stiffness of the optical trap. However, the experimental approach was not sensitive to the form of the force-dependent unbinding rate. We compare and contrast the predictions of the theoretical model with the experimental data in the presence and absence of catch bond, and the dependence of our theoretical results on the force scale f_m where the catch bond sets in.

For the current case of a cargo transported by a single motor, we first characterise the probability distribution of detachment forces obtained by our theoretical approach with the experimental data for two different values of the trap stiffness - $k_t = 0.01pN$ (Fig. 3a), and $k_t = 0.1pN$ (Fig. 3b) - for catchbonded and non catchbonded motors (Eq. 10). For low value of trap stiffness $k_t = 0.01pN/nm$ (Fig. 3a), corresponding to an experimentally observed stall force of $f_s = 0.9pN$, the theoretical probability distributions are largely insensitive to the catchbonded nature of dynein bond. Its worthwhile to point that, even for relatively low value of $f_m = 0.5pN(\sim f_s/2)$, the probability distribution of detachment force for the case of catchbonded motors is virtually indistinct with the probability distribution for non-catchbonded motors. This maybe understood in the following manner. When the trap stiffness is low, most of the unbinding events happen typically before the cargo attains a displacement which is larger than f_m which results in the theoretical probability distribution being virtually indistinguishable from the non-catchbonded case. The theoretical curves at this trap stiffness - both for the catchbonded and non-catchbonded cases - corresponding to the probability distribution exhibit broad qualitative agreement with the experimentally obtained distribution for this case. Note that in the experiments, only displacements greater than a certain threshold were recorded, implying that data was not available for very low detachment forces. This leads to a discrepancy between the observed and theoretical frequency distributions at very low detachment forces as seen in Fig. 3(a) and (b). Further, observed stall forces in experiments are distributed around the mean value, while the theoretical model has an unique stall force at a given trap stiffness. Thus, detachment forces greater than the stall force are not accessible in the theoretical curves, while it is possible to have detachment forces in the experiment greater than the *mean* stall force.

In contrast, for high values of the trap stiffness, ($k_t = 0.1pN/nm$), the theoretically obtained distribution for the non-catchbonded case exhibits significant divergence from the experimental curve, as shown in Fig. 3(b). In general the effect of increasing the trap stiffness, leads to the a rightward shift of the distribution function to higher values of forces. Inclusion of catchbond effect, with the catchbond setting in $f_m = 1.1pN(\sim f_s/2)$, results in improved quantitative agreement of the experimental probability distribution with the theoretical one. This in turn suggests that the catchbonded nature of dynein motors can indeed affect transport characteristics at high trap stiffness and needs to be accounted for.

Fig. 3(c) and Fig. 3(d) displays the theoretically obtained Cumulative distribution function (CDF) for range of trap stiffness for non-catchbonded and catchbonded case. As mentioned for the case of PDF, for low values of trap stiffness, the CDF for these two cases are virtually indistinguishable. On the other hand for high values of trap stiffness there are significant divergences in the nature of CDF for the two cases.

B. Cargo transport by multiple motors

For multiple motors, we explore the regime that $f_m = f_s$. A catchbond response can still be triggered in this regime, for multiple motors, as the cargo can be transported beyond the distance corresponding to the stall-force of one motor.

1. Catchbond alters transport properties

In Fig.4 we see a comparison between trajectories of a cargo carried by a maximum of 4 motors based on the presence or absence of catchbond. We observe in Fig. 4(a) that both detachment force distributions terminate at $\sim 4.4pN$ which corresponds to the detachment force $f_{max} = Nf_s$, the maximum possible force scale the cargo can reach to before all N motors are stalled. Although the detachment force distribution in case of slip bond (red curve) has a significant value in intermediate distances (in between $1.5 - 3.5pN$), the detachment force distribution for catchbond (blue and greens curves) is biased towards larger distances ($\gtrsim 4\ pN$) with visible characteristic peaks at intervals of $\sim 1.1pN$ (Fig.4(a)). These peaks correspond to the external force equal to multiples of stall force of a single motor. The bias towards larger unbinding forces is suggestive of the fact that catchbond helps the motors to tolerate a high load force by decreasing the unbinding rate of the motors and as a result, the cargo stays bound and moves further away from the trap center. A similar persistent nature for catchbond can be spotted from the comparison of First Passage time (FPT) distribution

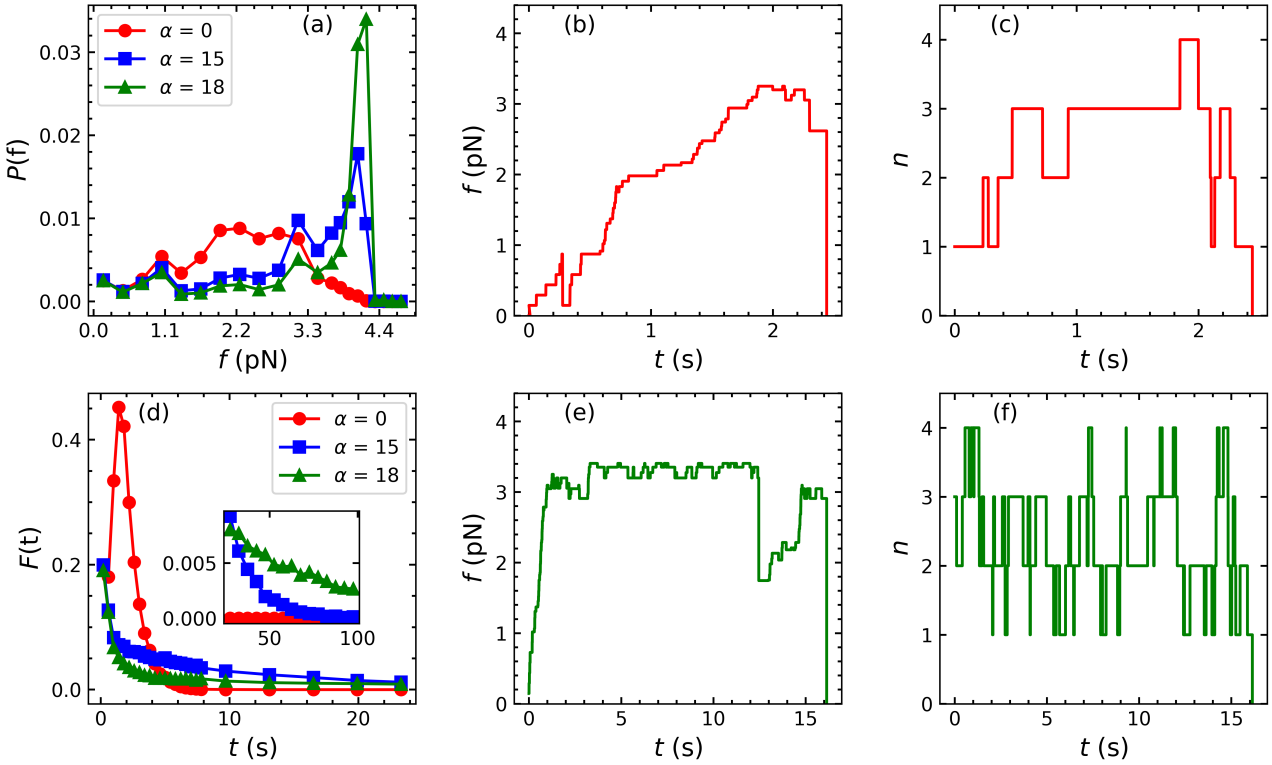

FIG. 4. Panels (a) and (d) show the normalized probability distributions for Detachment force f and First Passage time t respectively of the cargo for $N = 4$. Red curves correspond to slipbond ($\alpha = 0\ k_BT$) , blue curves to catchbond ($\alpha = 15\ k_BT$) and green curves to Strong catchbond ($\alpha = 18\ k_BT$). *The inset in panel (d) shows a magnified view of the distribution corresponding to longer time scales. Panels (b) and (e) show sample trajectories of the cargo in the absence and presence of catchbond respectively. Panels (c) and (f) show the corresponding trajectories of the cargo in state-space in the absence and presence of catchbond respectively. The parameter values used are as follows : $\pi_o = 1.6$ s^{-1}, $\epsilon_o = 0.27$ s^{-1}, $l_o = 55$ nm, $v_o = 362$ nm s^{-1}, $f_s = 1.1$ pN, $f_d = 0.67$ pN, $f_m = 1.1$ pN, $f_o = 7$ pN, $k_t = 0.02$ pN nm^{-1}.

curves for two cases (Fig.4(d)). While most of the runs terminate after smaller duration (about few seconds) for slipbond (red curve), the catchbond distributions (blue and green curves) have very long tails extending to larger timescales (a few minutes). The tail is longer for stronger catchbonded motors (higher α) as shown in Fig.4(d) (inset). Fig.4(b) and Fig.4(c) show a representative trajectory of the cargo for slipbonded motors in terms of instantaneous force on the cargo and number of motors attached to the filament (motor state of the cargo) as a function of time respectively while Fig.4(e) and Fig.4(f) depict the same for catchbonded motors. In higher motor states, the cargo can travel farther away from the trap-center and hence be subjected to a larger load force. As depicted in Fig. 4(c), in the slipbond case, this results in a rapid unbinding of motors as with each unbinding, the remaining motors take on a bigger share of load, exponentially increasing their tendency to unbind. However, in the catchbond case, beyond the threshold force (f_m) the unbinding rate decreases with increasing load. Thus catchbond helps the motors to stay bound in a higher load regime until unbound motors (if any) rebinds to the filament again. This results in frequent occurrence of cargo transitions from a lower to a higher motor state over the course of the cargo transport as depicted in Fig. 4(f).

2. *Motor Velocities and Binding/ Unbinding rates strongly affect cargo transport characteristics*

In an experimental context, the variation of free motor velocity (v_o) can be associated with the change in ATP concentration in the cell. Similarly the variation of binding and unbinding rates can be associated with introduction of promoting or inhibiting reagents that support or oppose the stability of the bond between the motor and the binding site on the microtubule [27, 29].

Similar to the case of a single motor, in multiple motor case also, the average FPT monotonically decays for increasing unbinding rate (Fig. 5(a)) while it monotonically increases with increasing binding rate (Fig. 5(b)). We also observe that the presence of catchbond (blue and green curves) causes the average first passage time

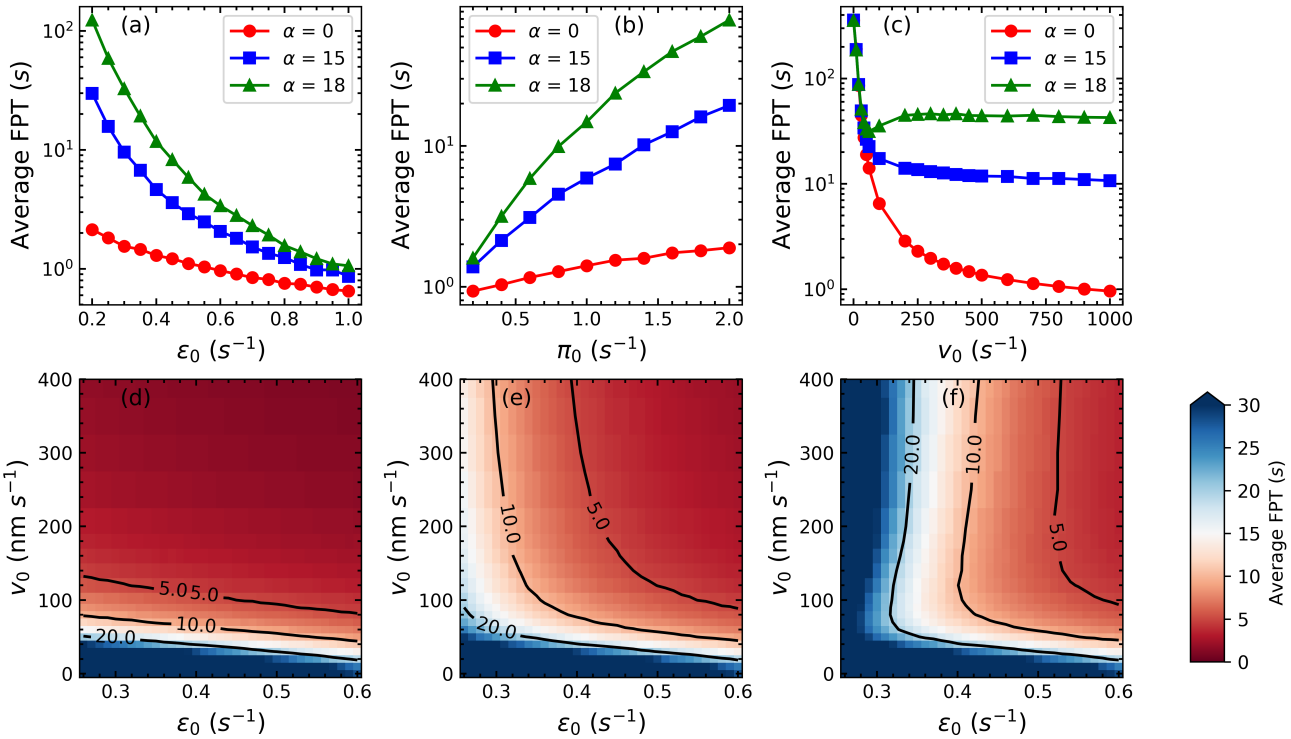

FIG. 5. (a) Average First Passage time (FPT) as a function of ϵ. (b) Average First Passage time as a function of π. (c) Average First Passage time as a function of v_o. Red corresponds to slipbond ($\alpha = 0k_BT$), blue to catchbond ($\alpha = 15\ k_BT$) and green to strong catchbond ($\alpha = 18\ k_BT$). Panels (d),(e) and (f) are contour plots of Average First Passage Time in the ϵ-v_0 plane, with slipbond ($\alpha = 0\ k_BT$), presence of catchbond ($\alpha = 15\ k_BT$) and strong catchbond ($\alpha = 18\ k_BT$) respectively. The parameters used are: N = 4, $\pi_o = 1.6$ s^{-1} (for varying ϵ_o), $\epsilon_o = 0.27$ s^{-1} (for varying π_o), $v_o = 362$ nm s^{-1}. $l_o = 55$ nm. $f_s = 1.1$ pN, $f_d = 0.67$ pN, $f_m = 1.1$ pN, $f_o = 7$ pN (Strong catchbond). $k_m = 0.2$ pN nm^{-1}, $k_t = 0.02$ pN nm^{-1}.

to differ by an order of magnitude than that of slipbond (red curve) for biologically relevant binding and unbinding rates.

As previously noted for single motor-driven cargo, higher velocities imply that the motors reach a higher load regime faster and thus become more prone to unbinding (Fig.5(c)) in case of a cargo transported by a team of dyneins. Therefore the average FPT associated with faster motors are lower than that of the slower motors. In the Fig.5(c), we observe a re-entrant behaviour in the average first passage time with increase in v_o for strong catchbond ($\alpha = 18$) (green curve). The average first passage time initially decreases with increasing v_o until it reaches a minimum at v_o ~70 $nm\ s^{-1}$ and then again starts to increase until v_o ~300 $nm\ s^{-1}$. Beyond $v_o \sim 300 nms^{-1}$ the average FPT decreases very slowly, in contrast to the single motor behaviour in Fig. 2(b) where the FPT saturates with velocity for the case of strong catchbond. The maximum can be ascribed to the threshold where the fraction of cargo trajectories undergoing catchbonded states is maximized. For even higher velocities the effect of catchbond remains the same. The lagging motors catch up to leading motors quickly thereby reducing the characteristic time-scale for superstall loads which trigger the catchbond. This leads to a very small decrease in the first passage time for very high motor velocity. Fig. 5(d-f) depicts contour maps of average first passage time in the $\epsilon - v_o$ plane under slipbond, catchbond ($\alpha = 15\ k_BT$) and strong catchbond ($\alpha = 18\ k_BT$) respectively. We observe that similar to Fig.5(c) (green curve) there is a re-entrant behaviour between $\epsilon = 0.25$ and 0.5 as we increase v_o (Fig.5(f)).

3. *Effect of changing number of motors*

Fig.6(a-b) shows that the average first passage time and average detachment force increase monotonically with the total number of motors (N). While the average detachment force in slipbond and catchbond is comparable for low motor numbers, catchbond values differ significantly from slipbond values for higher N reaching almost twice the value for N=7. It is noteworthy that the catchbond strengthens drastically as N increases. This is due to the fact that higher number of motors implies that the cargo can travel further

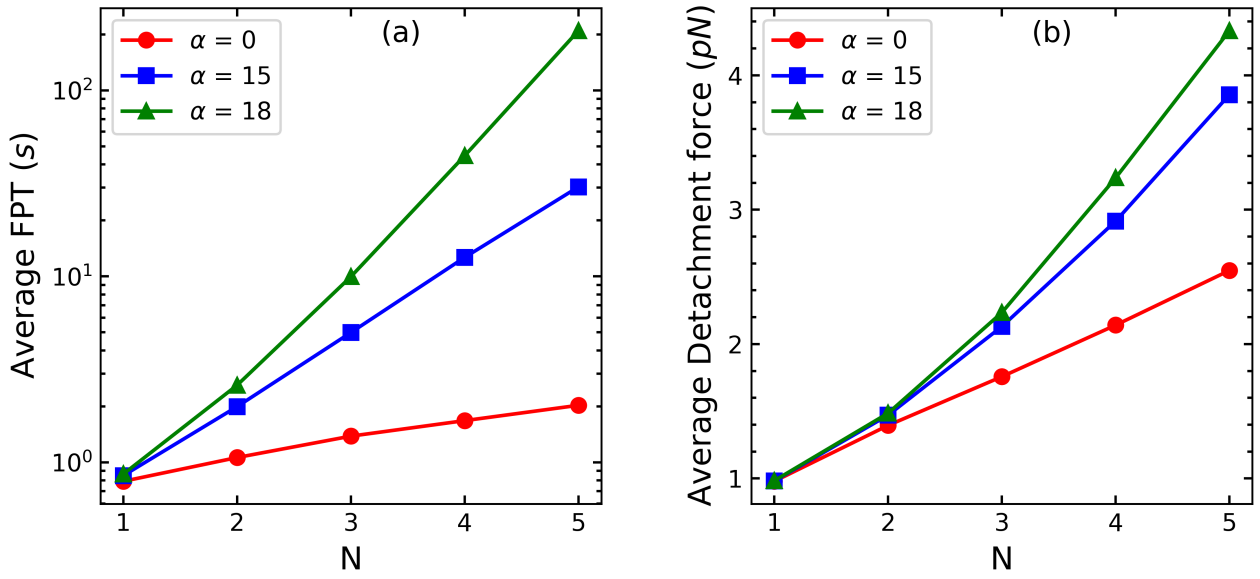

FIG. 6. (a) Average FPT as a function of total number of motors N. (b) Average Detachment force with varying N. Red corresponds to slipbond ($\alpha = 0k_BT$), blue corresponds to catchbond ($\alpha = 15k_BT$) and green with strong catchbond ($\alpha = 18k_BT$). The parameters used are : $\pi_o = 1.6$ s^{-1}, $\epsilon_o = 0.27$ s^{-1} , $v_o = 362$ nm s^{-1}. $l_o = 55$ nm. $f_s = 1.1$ pN, $f_d = 0.67$ pN, $f_m = 1.1$ pN, $f_o = 7$ pN. $k_m = 0.2$ pN nm^{-1} and $k_t = 0.02$ pN nm^{-1}.

away from the trap center before all motors are stalled, generating large external force. As motors progressively unbind, this high external load is shared among the remaining motors leading to large individual super-stall load and stronger catchbond. This is substantiated by the increase in the average first passage time by orders of magnitude with increase in N due to catchbond.

4. *Effect of variation of stall force*

The stall force of dynein is a well debated topic. While most experiments suggest that cytoplasmic dynein has a stall force of 1.1 pN [4, 22, 28], it has been reported that the stall force can be modified to $\sim$ 4 pN by complexing the dynein with dynactin and BicD2 (DDB complex) [30]. On the other hand dyneins found in yeasts are reported to have a very high stall force ($\sim$ 7 pN) [31, 32]. Fig.7(a) and Fig.7(b) show the variation of average first passage time and average detachment force respectively with increasing stall force (f_s). The average detachment force increases initially with f_s, reaches a maximum and then decreases with stall force in both schemes. The rise is seen to be steeper in the catchbond case (blue and green curves). As the average detachment force decreases, both slipbond and catchbond appear to converge gradually at higher f_s ($\gtrsim$ 2.5 pN). This indicates that since f_m increases with f_s, the likelihood of a motor achieving a catchbond state, drops with increasing f_s. This is also reflected in the average first passage time. Average FPT decreases rapidly with increasing f_s for both slipbond and catchbond and the curves converge at higher f_s. The decrease in average FPT with increasing f_s occurs due to the fact that velocity decreases less rapidly with higher f_s as given in Eq. 11, leading to further displacement from the trap centre resulting in larger load force. In all three cases, when there is greater binding affinity (lower unbinding rate or higher binding rate) it is apparent that for a smaller stall-force, there is a natural limitation on the distances that the cargo can travel. For larger stall-forces, individual motor velocities decrease less rapidly leading to motors travelling far faster and unbinding rapidly under the consequent load. In an intermediate regime, motors can travel farther and do not unbind as rapidly resulting in a marginally higher run-length (and hence detachment force). Catchbond exaggerates this effect by promoting further displacement by increasing the persistence of the cargo's bound state at higher loads. Catchbond, however, is triggered with a smaller likelihood with the increase of f_s and therefore, ceases to be of any aid beyond a certain force scale. This is apparent from how the three curves converge at $f_s \gtrsim 2.8pN$.

IV. DISCUSSION

While optical trap experiments have been a key tool to understand the transport properties of cellular cargo,

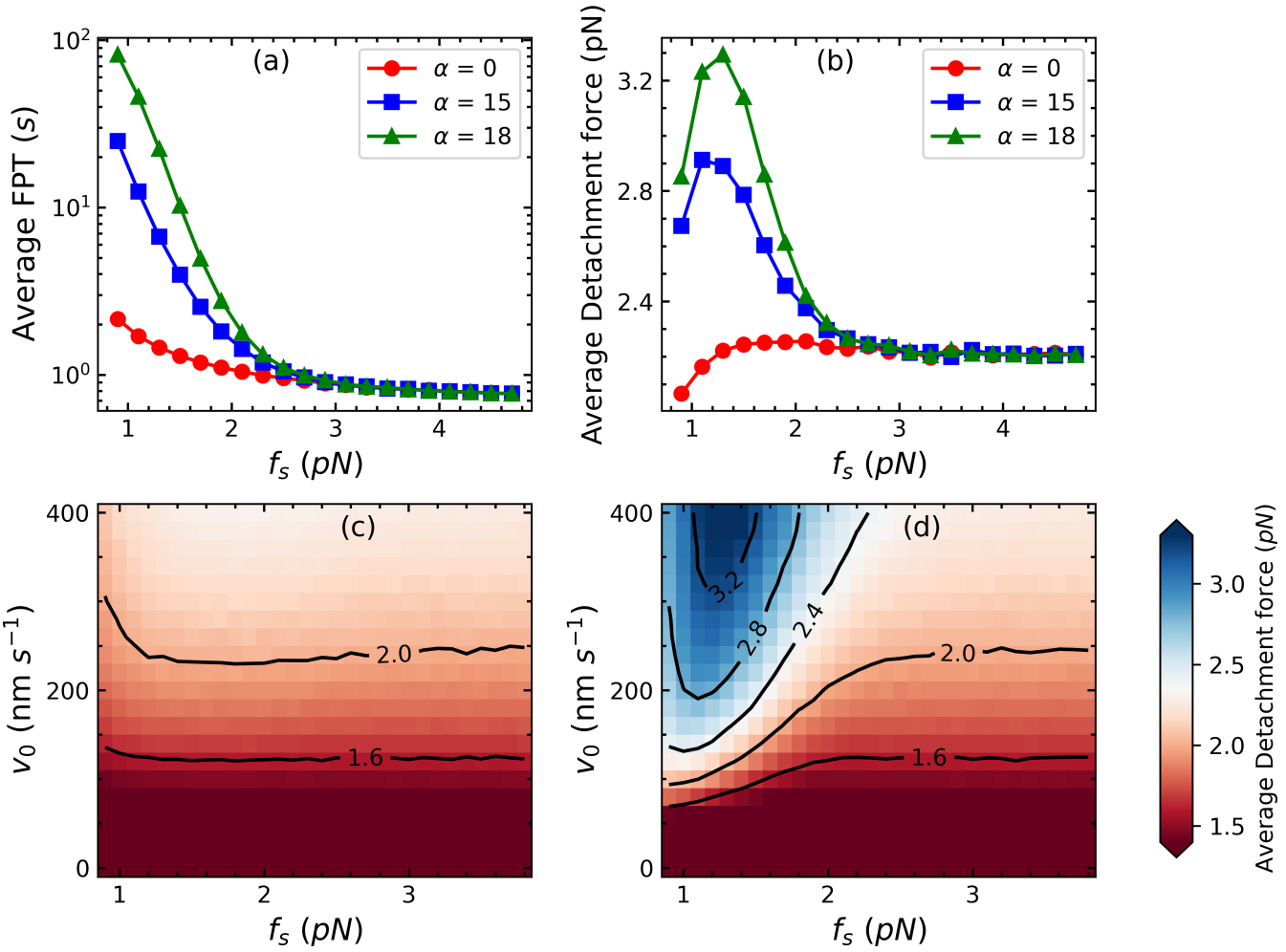

FIG. 7. Panels (a) and (b) shows the variation in Average FPT and Detachment force with stall force f_s. Panels (c) and (d) represent contour plots of Average Detachment force in the $f_s - v_o$ plane in the absence ($\alpha = 0\ k_BT$) and presence of catchbond ($\alpha = 18\ k_BT$) respectively. For panels (a) and (b), red, blue and green correspond to slipbond, catchbond and Strong catchbond respectively. The parameters used are: N = 4, $\pi_o = 1.6$ s^{-1} , $\epsilon_o = 0.27$ s^{-1} , $v_o = 362$ nm s^{-1}. $l_o = 55$ nm. $f_d = 0.67$ pN, $f_m = f_s$, $f_o = 7$ pN. $k_m = 0.2$ pN nm^{-1}, $k_t = 0.02$ pN nm^{-1}.

the properties of the catchbonded dynein motor protein in such a variable force assay has not been investigated theoretically.

In this paper we have first investigated the impact of catchbond behaviour on transport of a cellular cargo by a single molecular motor in an optical trap setting. We have contrasted our findings with the situation where the catchbond effects are absent. As expected, the prolonged lifetime due to catchbond leads to increased time of attachment of the cellular cargo to the microtubule. More revealingly, comparison with experimental data shows better qualitative and quantitative match for distribution of the detachment forces of the cargo being transported by single motor when catchbond behaviour of dynein is taken into account as opposed to the situation where the catchbond related effect is ignored. However it is worthwhile to point out that for the case of transport of cellular cargo by a single motor, the difference between catchbonded and non-catchbonded case manifests itself *only if*, catchbonding in the motor sets in at a force scale which is lower than the characteristic detachment force of the motor. While it can be argued, that on physical grounds these two force scales need not necessarily coincide, only a careful controlled experiment can shed more light on this ambiguity.

Next we have focused our attention on the collective manifestation of many catchbonded motors on the transport properties in such optical trap setting. With increase in motor number N, for the case of catchbonded dynein, there is a drastic increase in average FPT which grows roughly exponentially with N. In contrast, the corresponding increase of FPT with N for non-catchbonded motors is substantially more inhibited. We also find the catchbonding effect leads to sharper increase in the average detachment force of the cargo in the trap. Experiments performed with motor teams carrying single

phagosomes have demonstrated that while team of kinesin motors fail to work collectively under conditions of variable force setting of optical trap, team of dynein motors are not only able to counteract larger forces (due to the optical trap) but their tenacity is much more pronounced [18, 19]. Indeed the findings of our model are not only consistent with these experimental observations but importantly it elucidates the role of catchbond in fashioning these transport characteristics which delineates the difference between team of catchbonded motors (dynein) with team of non-catchbonded motors (kinesin).

Interestingly, we also observe a 're-entrant' like behaviour wherein, we find that average FPT of transported cargo initially decreases with decrease in motor velocity, before again increasing with the decrease in motor velocity both for the case of transport by single dynein and for the case of transport by multiple dynein motors. This is in contrast to the behaviour by non-catchbonded motors wherein, the average FPT monotonically decreases with increase in motor velocity. Note that various experiments have reported a wide range of dynein velocities from 49 nm/s [30] to 1200 nm/s [33]. Motor velocities are also known to depend sensitively on the ATP concentration [31, 34]. Further, the complexing of dynactin with dynein has been shown to cause a five to ten-fold increase of velocities [30]. Dynein motors can thus operate over a wide range of velocities and hence access this non-monotonic behaviour of FPT with change in velocity. Similarly, complexation of dynein with dynaction has been reported to cause a wide variation in the observed stall forces as well [30]. With this motivation we also study the variation of the average FPT with varying stall forces as well. We observe a non-trivial dependence of the average detachment force with the dynein motor stall force f_s. In particular we find that for certain parameter regime, on increasing the stall force f_s, the average detachment force initially increases before again decreasing at higher values of stall force.

Initial experiments on cytoplasmic dynein, with a measured stall force of $f_s = 1.1pN$ revealed that the catch bond set in at a force scale roughly equal to the stall force [20]. However the demonstration that this experimentally measured stall forces was in fact an artefact of the optical trap stiffness and in fact can vary with the trap stiffness until it reaches that true stall at $f_s \simeq 2pN$ [25] calls into question the force scale f_m at which the catchbond sets in. Catchbonding, generically, is thought to arise from allosteric deformations of the protein structure that in principle should be independent of the stall force. While the precise molecular mechanisms of the catchbond for dynein remain to be completely understood, a similar argument would imply a threshold force, f_m, for the activation of the catchbond is independent of the apparent stall force, and hence the trap stiffness. While catchbonding effects are difficult to distinguish for single motors, they should have non-trivial effects on the transport properties for cargo carried by multiple motors. Such multiple motor experiments at different trap stiffness can then show drastically different properties depending on the measured value of the mean stall forces, and can be used to measure the force scale at which the catchbonding sets in. While our results for the case of multiple motors assumes $f_s = f_m$, in line with previous work, future experiments with different trap stiffness can help elucidate the relevant force scales and help understand the molecular origins of the dynein catchbond.

AUTHOR CONTRIBUTIONS

NS carried out simulations, analyzed model and data and wrote manuscript, SG formulated and carried out theoretical calculations, analyzed model and data and wrote manuscript, MKM and SM designed study, analyzed model and data and wrote manuscript.

ACKNOWLEDGMENTS

SM acknowledges financial support and hospitality for visit to ICTP, Trieste under the Associateship program, where part of the work was done. Financial support is acknowledged by SM, NS and MKM for SERB project No. EMR /2017/001335. MKM and SG acknowledge financial support from IIT Bombay.

[1] B. Alberts, The cell as a collection of protein machines: preparing the next generation of molecular biologists, cell **92**, 291 (1998).

[2] M. A. Welte, S. P. Gross, M. Postner, S. M. Block, and E. F. Wieschaus, Developmental regulation of vesicle transport in drosophila embryos: forces and kinetics, Cell **92**, 547 (1998).

[3] J. Howard and R. Clark, Mechanics of motor proteins and the cytoskeleton, Appl. Mech. Rev. **55**, B39 (2002).

[4] M. A. Welte, Bidirectional transport along microtubules, Current Biology **14**, R525 (2004).

[5] N. P. Ferenz, R. Paul, C. Fagerstrom, A. Mogilner, and P. Wadsworth, Dynein antagonizes eg5 by crosslinking and sliding antiparallel microtubules, Current Biology **19**, 1833 (2009).

[6] S. Muhuri and I. Pagonabarraga, Lattice-gas model for active vesicle transport by molecular motors with opposite polarities, Physical Review E **82**, 021925 (2010).

[7] J. W. Driver, A. R. Rogers, D. K. Jamison, R. K. Das, A. B. Kolomeisky, and M. R. Diehl, Coupling between motor proteins determines dynamic behaviors of motor protein assemblies, Physical Chemistry Chemical Physics **12**, 10398 (2010).

[8] D. Bhat and M. Gopalakrishnan, Effectiveness of a dynein team in a tug of war helped by reduced load sensitivity of detachment: evidence from the study of bidirectional endosome transport in d. discoideum, Physical Biology **9**, 046003 (2012).

[9] S. A. McKinley, A. Athreya, J. Fricks, and P. R. Kramer, Asymptotic analysis of microtubule-based transport by multiple identical molecular motors, Journal of theoretical biology **305**, 54 (2012).

[10] S. Sutradhar and R. Paul, Tug-of-war between opposing molecular motors explains chromosomal oscillation during mitosis, Journal of theoretical biology **344**, 56 (2014).

[11] S. Chandel, A. Chaudhuri, and S. Muhuri, Collective transport of weakly interacting molecular motors with langmuir kinetics, EPL (Europhysics Letters) **110**, 18002 (2015).

[12] R. T. McLaughlin, M. R. Diehl, and A. B. Kolomeisky, Collective dynamics of processive cytoskeletal motors, Soft matter **12**, 14 (2016).

[13] P. Puri, N. Gupta, S. Chandel, S. Naskar, A. Nair, A. Chaudhuri, M. K. Mitra, and S. Muhuri, Dynein catch bond as a mediator of codependent bidirectional cellular transport, Physical Review Research **1**, 023019 (2019).

[14] S. Klumpp and R. Lipowsky, Cooperative cargo transport by several molecular motors, Proceedings of the National Academy of Sciences **102**, 17284 (2005).

[15] A. Nair, S. Chandel, M. K. Mitra, S. Muhuri, and A. Chaudhuri, Effect of catch bonding on transport of cellular cargo by dynein motors, Physical Review E **94**, 032403 (2016).

[16] D. Bhat and M. Gopalakrishnan, Transport of organelles by elastically coupled motor proteins, The European Physical Journal E **39**, 1 (2016).

[17] C. Leidel, R. A. Longoria, F. M. Gutierrez, and G. T. Shubeita, Measuring molecular motor forces in vivo: implications for tug-of-war models of bidirectional transport, Biophysical journal **103**, 492 (2012).

[18] A. K. Rai, A. Rai, A. J. Ramaiya, R. Jha, and R. Mallik, Molecular adaptations allow dynein to generate large collective forces inside cells, Cell **152**, 172 (2013).

[19] R. Mallik, A. K. Rai, P. Barak, A. Rai, and A. Kunwar, Teamwork in microtubule motors, Trends in cell biology **23**, 575 (2013).

[20] A. Kunwar, S. K. Tripathy, J. Xu, M. K. Mattson, P. Anand, R. Sigua, M. Vershinin, R. J. McKenney, C. C. Yu, A. Mogilner, *et al.*, Mechanical stochastic tug-of-war models cannot explain bidirectional lipid-droplet transport, Proceedings of the National Academy of Sciences **108**, 18960 (2011).

[21] M. Piel and P. T. Tran, Cell shape and cell division in fission yeast, Current Biology **19**, R823 (2009).

[22] W. O. Hancock, Bidirectional cargo transport: moving beyond tug of war, Nature reviews Molecular cell biology **15**, 615 (2014).

[23] S. Guha, M. K. Mitra, I. Pagonabarraga, and S. Muhuri, Novel mechanism for oscillations in catchbonded motor-filament complexes, Biophysical Journal **120**, 4129 (2021).

[24] K. G. Ohashi, L. Han, B. Mentley, J. Wang, J. Fricks, and W. O. Hancock, Load-dependent detachment kinetics plays a key role in bidirectional cargo transport by kinesin and dynein, Traffic **20**, 284 (2019).

[25] S. Brenner, F. Berger, L. Rao, M. P. Nicholas, and A. Gennerich, Force production of human cytoplasmic dynein is limited by its processivity, Science advances **6**, eaaz4295 (2020).

[26] H. Sakakibara, H. Kojima, Y. Sakai, E. Katayama, and K. Oiwa, Inner-arm dynein c of chlamydomonas flagella is a single-headed processive motor, Nature **400**, 586 (1999).

[27] R. J. McKenney, M. Vershinin, A. Kunwar, R. B. Vallee, and S. P. Gross, Lis1 and nude induce a persistent dynein force-producing state, Cell **141**, 304 (2010).

[28] R. Mallik, D. Petrov, S. Lex, S. King, and S. Gross, Building complexity: an in vitro study of cytoplasmic dynein with in vivo implications, Current Biology **15**, 2075 (2005).

[29] A. R. Chaudhary, F. Berger, C. L. Berger, and A. G. Hendricks, Tau directs intracellular trafficking by regulating the forces exerted by kinesin and dynein teams, Traffic **19**, 111 (2018).

[30] V. Belyy, M. A. Schlager, H. Foster, A. E. Reimer, A. P. Carter, and A. Yildiz, The mammalian dynein–dynactin complex is a strong opponent to kinesin in a tug-of-war competition, Nature cell biology **18**, 1018 (2016).

[31] S. Toba, T. M. Watanabe, L. Yamaguchi-Okimoto, Y. Y. Toyoshima, and H. Higuchi, Overlapping hand-over-hand mechanism of single molecular motility of cytoplasmic dynein, Proceedings of the National Academy of Sciences **103**, 5741 (2006).

[32] A. Gennerich, A. P. Carter, S. L. Reck-Peterson, and R. D. Vale, Force-induced bidirectional stepping of cytoplasmic dynein, Cell **131**, 952 (2007).

[33] J. L. Ross, K. Wallace, H. Shuman, Y. E. Goldman, and E. L. Holzbaur, Processive bidirectional motion of dynein–dynactin complexes in vitro, Nature cell biology **8**, 562 (2006).

[34] E. Hirakawa, H. Higuchi, and Y. Y. Toyoshima, Processive movement of single 22s dynein molecules occurs only at low atp concentrations, Proceedings of the National Academy of Sciences **97**, 2533 (2000).